Infinitely Divisible Cascades to Model the Statistics of Natural Images

Pierre Chainais, *Member*, *IEEE*

Abstract—We propose to model the statistics of natural images, thanks to the large class of stochastic processes called Infinitely Divisible Cascades (IDCs). IDCs were first introduced in one dimension to provide multifractal time series to model the so-called *intermittency phenomenon* in hydrodynamical turbulence. We have extended the definition of scalar IDCs from one to N dimensions and commented on the relevance of such a model in fully developed turbulence in [1]. In this paper, we focus on the particular 2D case. IDCs appear as good candidates to model the statistics of natural images. They share most of their usual properties and appear to be consistent with several independent theoretical and experimental approaches of the literature. We point out the interest of IDCs for applications to procedural texture synthesis.

Index Terms—Stochastic processes, picture/image generation, fractals, image processing and computer vision, statistical, image models.

1 Introduction

By "natural images," one usually means gray-level images from the real world. Statistical inference may be of great use in analyzing and understanding such images, for example, using Bayesian procedures for object tracking, pattern recognition, and analytical performance analysis. To this aim, there is a need for probabilistic models of natural images [2], [3], [4]. For instance, as far as object recognition is concerned, assuming the background is a Gaussian noise always yields underestimates of the probability of false alarm. Another motivation for pursuing image statistics has been to understand the architecture of animal visual systems. Efficient systems take advantage of statistical structure in their input signals aiming at both denoising and compact representation. Note that there is a large array of applications that benefit from the advances in modeling of image statistics: texture synthesis, image compression, image classification, image denoising, and so forth. In this context, an image is treated as a realization of a spatial stochastic process defined on some domain in $\mathbb{R}^2$. We emphasize that the purpose of such models is to capture the main common statistical features of a large class of images. In general, such models have no ambition to generate some realistic picture from a *single* stochastic process realization without any a priori information, even though they often provide us with methods for texture synthesis.

In this framework, let us first recall some usual assumptions commonly used in the statistical modeling of natural images. Despite the anisotropy of the real world due to gravity and the dissymmetry between the floor and the sky, models for natural images are usually assumed to be homogeneous and isotropic. Since this is not yet an easy task, to build such models, one can propose homogeneous and isotropic models to describe the statistics of natural images. Precisely, the processes presented below obey both true homogeneity and isotropy. Note that they can take inhomogeneity and anisotropy into account as well within rather soft limitations (see [1]). As already mentioned, it is commonly accepted [2], [3], [4], [6], [7], [8], [9], [10] that the power density spectrum of natural images follows a power law of the form $S(k) \propto 1/k^{2-\eta}$, which is a signature of the scale invariance property. For instance, a value of $\eta = 0.19$ was observed by Ruderman and Bialek [9]. It is also known that observed distributions are non-Gaussian. Peaked distributions with fat tails are reported in experimental works [2], [3], [4], [11], [12], [13], [14]. In contrast with a Gaussian process, which would be completely determined by its second-order statistics, higher order statistics have to be considered here. As a consequence, most of the difficulty encountered in the search for a relevant model comes from the fact that it should be *scale invariant*, as well as *non-Gaussian*. A candidate as a scale invariant Gaussian model could be the fractional Brownian sheet, a 2D extension of the fractional Brownian motion [15], [16]. However, applications call for more versatility so that there is actually a need for a larger family of non-Gaussian scale invariant models.

Thus, stochastic processes modeling natural images should be non-Gaussian scale invariant processes. Such properties appear as well in the statistical analysis of intermittency in turbulent fluid flows [1], [17], which motivated the multifractal formalism approach [18], [19], [20]. This analogy between turbulence and natural images was already proposed in previous works [4], [21]. In the works by Turiel et al. [21], [22], a multifractal analysis was carried out and the Extended Self-Similarity property [17], [23] was used. As a consequence, there are evidences that multifractal processes [20] could be good models for natural images. Note that the multifractal analysis can be embedded within the framework of *infinitely divisible scaling* [24], [25]. In this framework, the scale invariance property is associated to the power law scaling behavior of higher order moments of velocity increments in a turbulent flow. This behavior is connected to the description of the evolution of the probability

• *The author is with LIMOS UMR CNRS, University Blaise Pascal Clermont-Ferrand II, 63173 Aubière CEDEX, France. E-mail: pchainai@isima.fr.*

Manuscript received 27 Apr. 2006; revised 27 Oct. 2006; accepted 29 Jan. 2007; published online 13 Feb. 2007.
Recommended for acceptance by A. Srivastava.
For information on obtaining reprints of this article, please send e-mail to: tpami@computer.org, and reference IEEECS Log Number TPAMI-0330-0406.

Fig. 1. Examples of natural images from the van Hateren Data Basis [5].

density functions (pdfs) of velocity increments from Gaussian at a large scale to non-Gaussian at a small scale. We will see below that similar connections can be used for images. For instance, the scaling behavior of the moments of box-averaged intensities (respectively, wavelet coefficients) will describe the evolution of pdfs of box-averaged intensities (resp. wavelet coefficients) from large to small scales. The framework of infinitely divisible scaling [1], [24], [25], [26], [27] makes this connection explicit and gave hints to the construction of *infinitely divisible cascades* (IDCs).

Infinitely divisible cascades (IDCs) [28], [29], [30], [31], [32], [41] are a family of multifractal processes that were introduced in one dimension as a randomized version of the canonical multiplicative cascades by Mandelbrot [33]. Their definition has been extended from one dimension to N ($N \geq 2$) dimensions in [1], [34]. In two dimensions, IDCs provide us with a versatile model for images that has a power law spectrum ($\propto k^{-\alpha}$) and non-Gaussian distributions controlled by the choice of few parameters. Their scaling properties can be precisely prescribed as well. The main purpose of this article is to show that 2D IDCs appear as a very good candidate to model the statistics of natural images. Moreover, IDCs provide us with a tool for procedural texture synthesis so that many applications can be considered.

The paper is organized as follows: Section 2 recalls on multifractal analysis and multiplicative cascades and gives the main definitions and properties of IDCs. We will remark that IDCs meet most of the known properties of natural images listed above (for example, scale invariance and non-Gaussian distributions). Even the "mysterious" robustness of scaling properties to nonlinear transformations (for example, I, $\log I$, and $I^\alpha \ldots$) can be understood in this approach. Section 3 reviews and comments on several recent models of natural images. The IDC approach permits a better understanding of both experimental observations and theoretical models in a consistent framework. We shed some light on existing connections between IDCs and the description of the dependence of natural image statistics on the resolution by using a Fokker-Planck equation. We also comment on the link between IDCs and Gaussian scale mixtures (GSMs). We introduce the Bessel I forms as a subclass of IDCs of particular relevance. Section 4 reports on the statistical analysis of a set of natural images from the Van Hateren data basis [5] to illustrate the relevance of IDCs to model natural images. Finally, Section 5 reports on the versatility of IDCs for procedural texture synthesis, thanks to their many degrees of freedom. Some other possible applications are considered.

2 Infinitely Divisible Cascades in N Dimensions

2.1 Background

The purpose of this section is to recall on the necessary theoretical background about multifractal processes and multiplicative cascades to make this paper self-contained for the reader not familiar with such approaches.

2.1.1 Multifractal Processes

Scaling has been observed for many years in a large number of fields including natural phenomena: turbulence in hydrodynamics, rhythm of human heart in biology, spatial repartition of faults in geology, traffic in computer networks, financial markets, and so forth. The multifractal formalism [17], [20], [35] has become one of the most popular frameworks to analyze signals that exhibit *power law scaling*. For a one-dimensional (1D) process, this latter term refers to the power law behavior of the absolute moments of the increments $\delta_r X(x) = X(x+r) - X(x)$ of a process X. Then, the scaling behavior is described by a set of multifractal exponents $\tau(q)$ such that[1]

$$\mathbb{E}|\delta_r X(x)|^q \sim C_q r^{\tau(q)} \qquad \text{as } r \to 0, \tag{1}$$

where $\mathbb{E}$ denotes mathematical expectation. For instance, statistically self-similar processes such as fractional Brownian motions [36] with Hurst exponent H fit into this framework with $\tau(q) = qH$. When $X(x)$ is a non-negative process, it is rather considered as the density of a multifractal measure. Then, (1) must be written for the associated measure (the integral of the density) of intervals of size r. Doing so yields scaling laws of the form

$$\mathbb{E}\varepsilon_r(x)^q \sim C_q r^{\tau(q)} \qquad \text{as } r \to 0 \tag{2}$$

for box averages $\varepsilon_r(x) = \frac{1}{r}\int_{x-r/2}^{x+r/2} X(x')dx'$. The so-called multifractal formalism establishes conditions under which property (1) or (2) and a multifractal behavior are equivalent. When the multifractal formalism holds, the local regularity of the trajectories of the process (the multifractal spectrum) is fully characterized by the set of exponents $\tau(q)$. However, this framework is restrictive in at least two ways. First, in real-world applications, one is usually confined to observing power laws in a given range of scales $r_{min} \leq r \leq r_{max}$, which we then prefer to call *multiscaling* to distinguish it from multifractals. Multiscaling is usually considered as the best approximation to (1) or (2) and as the first step toward the use of the multifractal formalism. However, although (1) and (2) are sensitive to the limiting behavior only, it may not capture some richness in the progression at all observable scales. Second, exact power laws may not provide an accurate description of the scaling behavior of data or models.

The need for an appropriate mathematical framework substituting (1) was met with the *infinitely divisible scaling* [1], [24], [25], [26], [27]. This setting allows for more flexible

1. A definition which works for any process is $\tau(q) = \liminf_{r\to 0} \log_r \mathbb{E}|\delta_r X(x)|^q$.

scaling and, thus, better fitting of data and honors the contribution of all scales in a range of interesting scales $r_{min} \leq r \leq r_{max}$ as follows:

$$\mathbb{E}|\delta_r X(x)|^q = C_q \exp[-\tau(q)n(r)],\ r_{min} \leq r \leq r_{max}, \qquad (3)$$

where $n(r)$ is some monotonic function. The infinitely divisible scaling framework generalizes (1), which is recovered by choosing $n(r) = -\ln r$. Such a behavior is analyzed in terms of a *cascading mechanism* through the scales from r_{max} to r_{min}, whereas the multifractal analysis applies to any process (see footnote 1) and is concerned with local properties in the limit of fine scales but not finite scales. Note that both multifractal analysis and infinitely divisible scaling can be formulated using wavelet coefficients [26], [27], [37], [38].

Although analysis tools for multiscaling processes have been widely developed for a long time, tools for synthesis of processes with prescribed and controllable infinitely divisible scaling have been proposed only recently [1], [28], [29], [30], [31], [32], [39], [40], [41]. Multiplicative cascades have always played a central role to this purpose in intimate connection with multifractals.

2.1.2 From Multiplicative Cascades to Infinitely Divisible Cascades

The ingredient common to cascades is an underlying multiplicative construction that is iterated through the scales. The *canonical binomial cascade* as introduced by Mandelbrot [33], [42] may be viewed as the archetype of multifractal random measures. It can be defined via the iterative products

$$\beta_n(x) = \prod_{\{(j,k):1\leq j\leq n, x\in I_{j,k}\}} W_{j,k} = \beta_{n-1}(x) \prod_{\{k:x\in I_{n,k}\}} W_{n,k}. \qquad (4)$$

Here, $I_{j,k}$ stands for the nested dyadic intervals $[k2^{-j}, (k+1)2^{-j})$ and $W_{j,k}$ denotes independent and identically distributed (i.i.d.) positive random variables of mean one ($\mathbb{E}W_{j,k} = 1$). By construction, β_n is constant over each interval $I_{n,k}$. By considering the β_n as densities, one can study their distribution functions $X_n(x) = \int_0^x \beta_n(u)du$. As positive martingales, these converge weakly to a limiting measure X [43], [44], which exhibits self-similarity and a multifractal behavior in the form of (1). Attractive from a signal processing point of view is the iterative aspect of (4), which allows for fast tree-based synthesis algorithms. This underlying tree structure is inherited from the nested arrangement of the $I_{j,k}$, which may be represented by the points $((k+1/2)2^{-j}, 2^{-j})$ in the (space,scale)-plane, see Fig. 2a. However, such cascades have two major drawbacks. They are *not strictly stationary* since the construction is not time-shift invariant; this may result in "blocking effects." Further, by construction, the scaling of moments is log2-periodic and favors the scale ratio equal to 2. In particular, self-similarity is only approximate since it is obeyed for dilations by a factor 2^n only.

Following a more recent idea by Barral and Mandelbrot [28], one may overcome both drawbacks by replacing the rigid nested arrangement of multipliers $W_{j,k}$ of the binomial cascade by a planar Marked Poisson point process $\{(x_i, r_i, W_i)\}_i$ where 1) the x_i are i.i.d. uniformly distributed on $\mathbb{R}$ with density 1, 2) the r_i are i.i.d. random variables on (0, 1) with density $1/r^2$; and 3) the W_i are i.i.d. positive random variables. This leads to the *Multifractal Product of Cylindrical Pulses* (MPCP), also called *compound Poisson cascades* (CPCs)—see Fig. 2b. More precisely, introducing the cone $\mathcal{C}_\ell(x) = \{(x', r') : \ell \leq r' \leq 1, x - r'/2 \leq x' < x + r'/2\}$, the CPC reads as

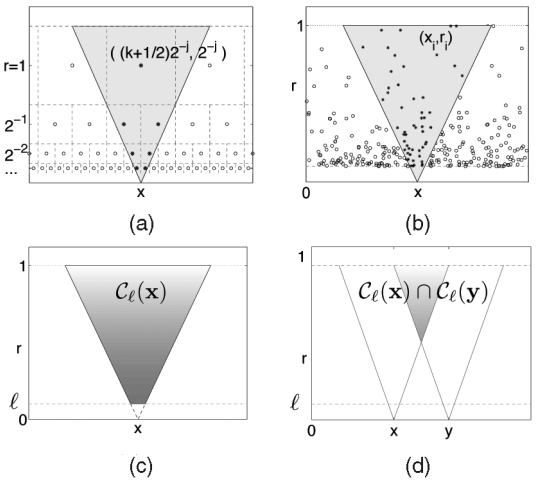

Fig. 2. **"Time-scale" construction of multiplicative cascades**. (a) Nested dyadic tree geometry behind the binomial cascade. (b) Stationary discrete geometry behind the CPC. (c) Stationary continuous geometry behind the IDC. The shaded cone indicate the region that determine the value of the cascade at location x. (d) The dependence between $Q_\ell(x)$ and $Q_\ell(y)$ stems entirely from the measure of the intersection of two cones $\mathcal{C}_\ell(x)$ and $\mathcal{C}_\ell(y)$.

$$\tilde{Q}_\ell(x) = \prod_{(x_i,r_i)\in\mathcal{C}_\ell(x)} W_i, \qquad Q_\ell(x) = \frac{\tilde{Q}_\ell(x)}{\mathbb{E}[\tilde{Q}_\ell(x)]}. \qquad (5)$$

Note that the binomial cascade uses similarly all multipliers $W_{j,k}$ such that $((k+1/2)2^{-j}, 2^{-j}) \in \mathcal{C}_{2^{-j}}(x)$. To obtain simple power law scaling for the CPC, one ensures that each "frequency band" of scales over the octave between 2^{-j-1} and 2^{-j} contributes on the average the same number of multipliers to $Q_\ell(x)$. This choice yields an expected number of Poisson points in $\mathcal{C}_\ell(x)$ proportional to $-\log \ell$, just as for binomial cascades. Then, true stationary multifractal measures are built, which obey power law scaling in the form of (2), where $\varepsilon_r(x) = \int_{x-r/2}^{x+r/2} Q_\ell(x')dx'$.

The N-dimensional version of CPC defined below results from a natural generalization of the 1D definition [1], see Fig. 3a: The intensity of the Poisson point process $(\mathbf{x}_i, r_i)$ is then described by the control measure $dm(\mathbf{x}, r) = cd\mathbf{x}dr/r^{N+1}$ on the space-scale half-plane $\mathcal{P}^+ := \mathbb{R}^N \times \mathbb{R}^+$ such that $m(\mathcal{C}_\ell) = \log(1/\ell)$. The choice $m(\mathcal{C}_\ell) = \log(1/\ell)$ ensures scale invariance. Note that the large scale in the definition of $\mathcal{C}_\ell(\mathbf{x})$ has been arbitrarily set to 1 without loss of generality so that resolution ℓ belongs to $(0, L = 1]$. Choosing a large-scale $L \neq 1$ reduces to a change of units $(\mathbf{x}, r) \to (\mathbf{x} \cdot L, r \cdot L)$. Moreover, to extend the class of images to be synthesized, this definition may be generalized by introducing some localized integration kernel[2] $f(\mathbf{x}) \neq \mathbb{1}_{[-1/2,1/2]}(\mathbf{x})$ in (5)

2. This may rejoin the *random wavelet expansions* evoked in [10].

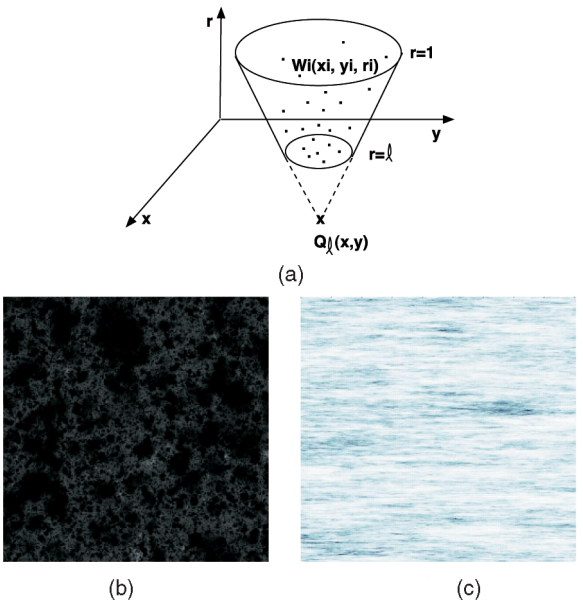

Fig. 3. (a) Space-scale cone defining $Q_\ell(\mathbf{x})$ at $\mathbf{x}(x,y)$. For a CPC, Q_ℓ is the product of those random multipliers $W_i(x_i,y_i,r_i)$ that belong to the cone $\mathcal{C}_\ell(\mathbf{x})$. (b) and (c) Examples of CPC using different integration kernels: (b) $f(\mathbf{x})=\cos(\pi\|\mathbf{x}\|)$ for $\|\mathbf{x}\|\in(-1/2,1/2)$ and 0 elsewhere; (c) $f(\mathbf{x})=\cos(\pi\sqrt{(x_1/a)^2+(x_2/b)^2})$ for $\|\mathbf{x}\|\in(-1/2,1/2)$ and 0 elsewhere, which introduces an anisotropic elliptical shape in the synthesis.

$$Q_\ell(\mathbf{x})=\frac{\prod_i W_i^{f\left(\frac{\mathbf{x}-\mathbf{x}_i}{r_i}\right)}}{\mathbb{E}\left[\prod_i W_i^{f\left(\frac{\mathbf{x}-\mathbf{x}_i}{r_i}\right)}\right]}. \tag{6}$$

The integration kernel f will play the role of some geometrical object in the image. This definition (6) may also be useful to attenuate small-scale discontinuities or to take into account some geometrical features of the images under study, see Figs. 3b and 3c. General definitions and mathematical results are recalled in the Appendices (which can be found at http://computer.org/tpami/archives.htm). An algorithm for synthesis is described in [1].

Noting that compound Poisson distributions are infinitely divisible and that

$$\ln Q_\ell(\mathbf{x})\propto\ln\left(\prod_{(\mathbf{x}_i,r_i)\in\mathcal{C}_\ell(x)}W_i\right)=\sum_{(\mathbf{x}_i,r_i)\in\mathcal{C}_\ell(\mathbf{x})}\ln W_i \tag{7}$$

one may read the right-hand term above as a specific (discrete) case of a random measure $M(\mathcal{C}_\ell)$ of the set $\mathcal{C}_\ell(\mathbf{x})$. This leads to the general definition of an IDC $Q_\ell(\mathbf{x})$ based on the summation of an infinitely divisible random measure $dM(\mathbf{x},r)$ (see Appendices (which can be found at http://computer.org/tpami/archives.htm) or, for example, [1] for definitions)

$$Q_\ell(\mathbf{x})=\frac{\exp\int f\left(\frac{\mathbf{x}-\mathbf{x}'}{r'}\right)\,dM(\mathbf{x}',r')}{\mathbb{E}\left[\exp\int f\left(\frac{\mathbf{x}-\mathbf{x}'}{r'}\right)\,dM(\mathbf{x}',r')\right]}, \tag{8}$$

where $M(\mathcal{C}_\ell)$, see Fig. 2c, is a random variable distributed by some infinitely divisible distribution G on $\mathbb{R}$ with moments generating function $\tilde{G}(q)=\exp[-\rho(q)m(\mathcal{C}_\ell)]$. Possible choices for distribution G are the Gaussian distribution, Poisson and compound Poisson distributions, Gamma and stable laws, and so forth. This is basically the most general definition of an *Infinitely Divisible Cascade* (IDC). IDCs can be seen as generalized continuous multiplicative cascades.

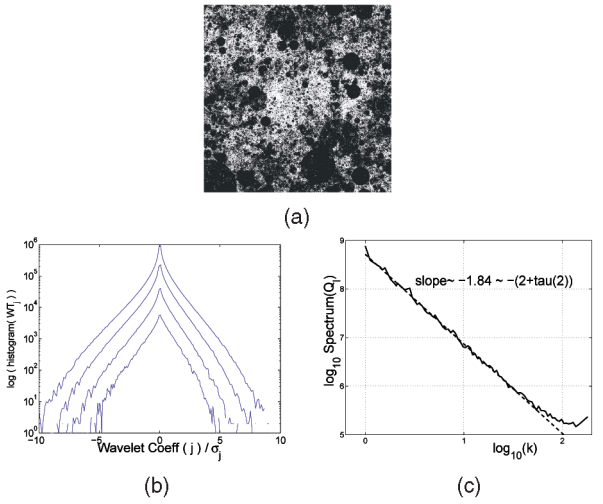

Fig. 4. (a) Example of a realization of a CPC Q_ℓ (gray levels) with $\tau(2)\simeq-0.16$—see (12) about the role of $\tau(2)$. (b) Estimated (log) histograms of normalized wavelet coefficients at various octaves j: they are all clearly non-Gaussian (Gaussian $\Rightarrow$ parabola). (c) Power law spectrum of $Q_\ell(\mathbf{x})$ as a function of $k=\|\mathbf{k}\|$ over two decades: the observed slope is prescribed by the choice of $\tau(2)$.

Among the full generality of infinitely divisible cascades, the family of compound Poisson cascades (CPC) [28] plays a special role for both historical and practical reasons. CPCs have been widely used to describe the statistics of turbulent flows [17], and they are easy to synthesize numerically [31]. Note that a Gaussian cascade is infinitely divisible but does not belong to the family of CPCs since the Gaussian distribution is not a compound Poisson distribution [45]. We will mostly focus below on CPCs as given by (6).

2.2 Properties

2.2.1 Homogeneity and Isotropy

An immediate consequence of the definition is that Q_ℓ is a *stationary/homogeneous positive random process* with the normalization $\mathbb{E}Q_\ell=1$. *Stationarity* is ensured by the invariance to translations of both the control measure $dm(\mathbf{x},r)$ and the cone of influence $\mathcal{C}_\ell(\mathbf{x})$. The symmetry of the cone's shape generates an *isotropic* structure as well. Some anisotropy may be obtained by choosing some anisotropic integration kernel $f(\mathbf{x})$.

2.2.2 Log-Infinitely Divisible Distribution

When f is a constant cylindrical pulse,[3] $Q_\ell(\mathbf{x})$ has a *log-infinitely divisible distribution*. In other words, $Y=\log Q_\ell$ has an infinitely divisible distribution $G_\ell(Y)$ described by its moment generating function $\tilde{G}_\ell(q)=\exp[-\varphi(q)m(\mathcal{C}_\ell)]$, where $\varphi(q)=\rho(q)-q\rho(1)$; recall that the function $\rho(q)$ is associated to the infinitely divisible random measure $dM(\mathbf{x},r)$ in (8). For instance, Q_ℓ might be log-Normal with $\rho(q)=\mu q+\frac{\sigma^2}{2}q^2$ and $\varphi(q)=\frac{\sigma^2}{2}q(1-q)$. For a CPC, $G_\ell(Y)$ is a compound Poisson distribution: The Poisson distribution

3. $f(\mathbf{x})=1$ on the disk of radius $1/2$ and zero elsewhere.

associated with the point process $(\mathbf{x}_i, r_i)$ is compound with the distribution of the logarithm of the i.i.d. random multipliers $\log W_i$. In this case, $\varphi(q) = 1 - \mathbb{E}W^q + q(\mathbb{E}W - 1)$. Departures from the normal law are visible on the histograms of wavelet coefficients at various scales as well, see Fig. 4b.

2.2.3 Scaling

Power law scaling behaviors are intimately connected to the particular choice of the control measure [1], [29], [31], [32], [46]

$$dm(\mathbf{x}, r) = \frac{dr}{V_{1/2} r^{N+1}} d\mathbf{x}, \tag{9}$$

where $V_{1/2}$ is the volume of the sphere of radius $1/2$ in N dimensions (for example, $dm(\mathbf{x}, r) = 4/\pi r^3 dr d\mathbf{x}$ in 2D). Then, $m(\mathcal{C}_r) = -\log r$ so that turning to local averages over a spherical volume V_r, $\varepsilon_r(\mathbf{x}) = \frac{1}{V_r}\int_{\|\mathbf{x}'-\mathbf{x}\|<r} Q_\ell(\mathbf{x}')\, d\mathbf{x}'$, one gets

$$\mathbb{E}[Q_\ell(\mathbf{x})^q] = \exp[-\varphi(q)\, m(\mathcal{C}_\ell)] = \ell^{\varphi(q)}, \tag{10}$$

$$\mathbb{E}\varepsilon_r(\mathbf{x})^q \sim r^{\tau(q)} \text{ for } r \ll 1, \tag{11}$$

where $\varphi(q) = \rho(q) - q\rho(1)$, and $\tau(q) = \varphi(q)$ at least within some limited range of values of q [1], [47], or $\tau(q) = \int \varphi(qf(\mathbf{x}))d\mathbf{x}$ in the most general case from (8) (if the integral converges, see Proposition 2.6 in [48]). Note the different status of $Q_\ell(\mathbf{x})$, which is a local quantity, and $\varepsilon_r(\mathbf{x})$, which is a space-averaged quantity. We emphasize that not only second-order statistics but also higher order statistics are prescribed as well. Note that these scaling behaviors are robust in a certain sense since they are preserved when elevating Q_ℓ to some power $\alpha > 0$, which corresponds to a nonlinear gamma correction. The multifractal formalism [19], [20] tells us that these scaling behaviors can be equivalently interpreted in terms of the regularity of $Q_\ell(\mathbf{x})$. A trivial constant image $Q_\ell(\mathbf{x}) = 1$ corresponds to $\tau(q) = 0$ for all q. On the contrary, the more $\tau(q)$ is nonlinear, the less regular is $Q_\ell(\mathbf{x})$, and the widest is the class of singularities in Q_ℓ. This ability of IDC to capture a wide class of regularity is valuable as far as the modeling of natural images—with textures and edges—is concerned.

2.2.4 Correlations

Turning to autocorrelation functions, one has at small scales [1]

$$\mathbb{E}[Q_\ell(0)Q_\ell(\mathbf{x})] \propto |\mathbf{x}|^{\tau(2)} \text{ for } |\mathbf{x}| \ll 1, \tag{12}$$

where 1 is the largest scale where the cascade begins. As a classical consequence of the multiplicative construction, one also has [1], [29], [31], [49]

$$\operatorname{cov}(\log Q_\ell(0), \log Q_\ell(\mathbf{x})) \propto \varphi''(0) \log|\mathbf{x}| \text{ for } |\mathbf{x}| \ll 1. \tag{13}$$

2.2.5 Power Law Spectrum

The behavior of correlation functions above is consistent with the observation of a power law spectrum (defined as the squared modulus of the Fourier transform) for both processes Q_ℓ and $\log Q_\ell(\mathbf{x})$. For $I(\mathbf{x})$, a *power law spectrum* $\propto k^{-(2+\tau(2))}$ with $\tau(2) < 0$ is expected, whereas a $\propto k^{-2}$ spectrum is expected for $\log I(\mathbf{x})$ (for example, see the appendix in [8] by Ruderman)—see Fig. 4c. This is a desired property for the modeling of natural images.

As a consequence, the scale invariance property (at least considered as the presence of a power law spectrum) can be observed both on Q_ℓ and $\log Q_\ell$. This remark is of particular relevance when dealing with the statistical modeling of the intensity $I(\mathbf{x})$ of natural images or of its logarithm $\log I(\mathbf{x})$. With little paradox, both quantities may display power law correlations and, therefore, a power law spectrum (see, for example, Section *Calibration invariance* in [8]).

3 IDC versus Some Existing Models

We have seen that IDCs provide us with a large class of *non-Gaussian scale invariant models*, with a precise control of their scaling properties and probability densities. Moreover, using (8), geometrical degrees of freedom may be introduced as well; these are studied elsewhere [1] and can be used for texture synthesis (see Section 5). In this section, we first comment on the ingredients that 2D IDCs share with several existing models of natural images. At this point, let us remark that the human eye is roughly a logarithmic sensor [50], which means that if I is the image intensity, the eye is roughly sensitive to $\log I$. Consequently, we will propose to use *multiplicative* models for the intensity of an image $I(\mathbf{x})$ ($\equiv Q_\ell(\mathbf{x})$) or, equivalently, *additive* models for the contrast $\phi(\mathbf{x}) \propto \log I(\mathbf{x})$ ($\equiv \log Q_\ell(\mathbf{x})$). We mainly focus on recent models proposed in [10], [13], [51], [52], [53], [54], [55], and [56]. We also show how IDCs give a way to the description of the distributions of an image observed at various resolutions, thanks to a Fokker-Planck equation. Finally, we introduce an interesting subclass of IDC models that we propose to call Bessel I forms.

3.1 Mumford and Gidas Infinitely Divisible Model

The approach proposed by Mumford and Gidas in [10] shares a lot of properties and assumptions with the 2D IDCs, which were initially built for the modeling of turbulent flows [1], [29], [31], [41]. However, we claim that the IDC framework brings new insights and perspectives to the modeling of natural images. Let us comment on the mathematical and axiomatic approach to the modeling of natural images proposed by Mumford and Gidas in [10]. According to these authors, relevant models should be non-Gaussian, display scale invariance, and make use of the infinitely divisible distributions family. IDCs precisely fulfill all these constraints in two dimensions (or even in $N \geq 2$ dimensions). Mumford and Gidas also suggest the use of a $1/r^3$ distribution of scales exactly like in the chosen control measure $dm(\mathbf{x}, r) \propto 1/r^3$. This power law distribution has strong connection to scaling properties. Only the choice $dm(\mathbf{x}, r) \propto r^{-3}$ ensures power laws multiscaling. This link was studied in details for 1D IDCs in [29], [31], [32] and for the dead leaves models in [8], [51], [57]. However, other choices might be considered that lead to the so-called "extended self-similarity" (ESS) previously introduced in turbulence [21], [23], [31], [32].

Such assumptions have quantitative consequences on distributions and correlations as well. For instance, a crucial property of natural images is that the covariance $C_I(\mathbf{x}_1, \mathbf{x}_2)$ of the intensity I ($\equiv Q_\ell$) obeys a power law $C_I(\mathbf{x}_1, \mathbf{x}_2) \propto |\mathbf{x}_2 - \mathbf{x}_1|^{-\beta}$. This is a consequence in the real space of the power spectrum in the Fourier space. Precisely, one of the initial motivation of the construction of IDC was to obtain power law correlations $\mathbb{E}[Q_\ell(0)Q_\ell(\mathbf{x})]$—see (12) and Fig. 10.

Only few models are able to reproduce so precisely the two-points-correlation structure of natural images—see [8], [14], [58], [57] (Fig. 10) where a dead leaves model is proposed. Furthermore, a usual property of multiplicative cascades is that the covariance $C_{\log I}(\mathbf{x}_1, \mathbf{x}_2)$ of the logarithm of intensity $\log I$ behaves as $\log \|\mathbf{x}_2 - \mathbf{x}_1\|$, see (13) and Fig. 10. Such property was used as a starting point to model the intensity I (not $\log I$) by Mumford and Gidas [10] since it is connected to scale invariance and rotational symmetry. We emphasize that this property receives some intuition in the framework of multiplicative cascades. Indeed, $\log \|\mathbf{x}_2 - \mathbf{x}_1\|$ simply reads as *the average number of common ancestors* $\{W_i, (\mathbf{x}_i, r_i) \in \mathcal{C}_\ell(\mathbf{x}_1) \cap \mathcal{C}_\ell(\mathbf{x}_2)\}$ of the respective values of $I(\mathbf{x}_1) \equiv Q_\ell(\mathbf{x}_1)$ and $I(\mathbf{x}_2) \equiv Q_\ell(\mathbf{x}_2)$.

At this point, note that Mumford and Gidas' model for the intensity I is similar to an additive log-IDC model that we would rather propose to model $\log I$ not I. We suggest to use a multiplicative model for the intensity I and an additive model for its logarithm $\log I$ within the consistent framework of IDC. Former works have usually focused separately on I or $\log I$ only. Within the IDC framework, the links between properties observed on I and $\log I$ are made explicit, thanks to the great amount of existing work by mathematicians, as well as physicists, on multifractal processes. Up to our knowledge, no other framework has been clearly proposed that considers the statistical properties of both I and $\log I$ in such a consistent manner.

Eventually, the notion of *clutter* is given a rather precise meaning in [10] by using infinitely divisible distributions. This notion of clutter becomes even clearer in the framework of IDC since it can be identified in a quantitative manner to $\log(1/\ell)$ (ℓ is the resolution of an IDC), which is the average number of multipliers W_i used to get $Q_\ell(\mathbf{x})$: The smaller the ℓ is, the larger the range of scales in the image and the larger the clutter. The quantity $\log(1/\ell)$ ($\ell < 1$) is usually called the *depth* of the cascade. More precisely, the cascade Q_ℓ can be decomposed here in as many successive "subcascades" as wanted by iterating the relation $Q_\ell = Q_{\ell'} \cdot Q_\ell^{\ell'}$, where $Q_\ell^{\ell'}$, $\ell < \ell'$, is built using truncated cones $\mathcal{C}_\ell^{\ell'}$ in the range $\ell \leq r \leq \ell'$.

3.2 A Basic Physical Interpretation of CPC

Among the whole family of IDC, CPCs are the most comfortable to work with since they receive some intuitive physical interpretation as far as the modeling of images is concerned. Indeed, taking the logarithm in (6), we get

$$\log Q_\ell(\mathbf{x}) = \sum_i \log W_i \cdot f\left(\frac{\mathbf{x} - \mathbf{x}_i}{r_i}\right) + K. \qquad (14)$$

Thus, the process $Q_\ell(\mathbf{x})$ can be interpreted as the intensity $I(\mathbf{x})$ resulting from the scattering of light by a random superposition of transparent cylinders of sizes $\{r_i\}$ placed above positions $\{\mathbf{x}_i\}$ and with i.i.d. random transparency W_i. This simplistic description points to the resemblance between CPCs and other classical approaches in image modeling where elementary objects of random sizes are distributed in space following a Poisson point process [2], [59]. In contrast with the dead leaves models, no occlusion is considered here. Note that, beyond 2D IDCs, one may also propose to use a 3D IDC model and then study its 2D projections.

Another interesting phenomenology can be proposed in the spirit of the recent work by Geusebroek [53], [54]. In this approach, the incident light on an optical sensor (for example, human eye and camera) is described as the result of a series of multiple reflections and diffractions by objects in an enlightened 3D space. The measured intensity $I(\mathbf{x})$ would be modeled as the product of the intensity of a source of light by the product of a random number of random multipliers (attenuation factors). In brief, the idea is that light coming from the source (for example, the sun) is affected by multiple reflections on macroscale objects, as well as by interreflections, due to the microscopic roughness of objects before it reaches the optical sensor (for example, a camera). Only a fraction of light is reflected at each interaction. This is one more approach that naturally leads to multiplicative cascades. Furthermore, Geusebroek implicitly suggests that an analysis in terms of infinitely divisible scaling may be relevant when he refers to the seminal paper by Castaing and Dubrulle [24]. In summary, approaches based on the physical modeling of natural images seem to naturally point to IDC.

3.3 Transported Generator Models (TGMs) and Bessel K Forms

Written in the form of (14), CPCs look quite similar to the TGMs proposed by Grenander and Srivastava in [13] and [52]. These authors have shown that a well-chosen random distribution of the profiles of random objects, the generators, could capture the variability of different types of scenes with very few free parameters.

We briefly recall below the main ingredients of the TGM, as described in [52]. This model assumes that

1. the a_i are i.i.d. standard normal,
2. the scales ρ_i are i.i.d. uniform on the interval $[0, L]$,
3. the locations $\mathbf{x}_i$ are samples from a homogeneous 2D Poisson process, with intensity $\lambda > 0$, and
4. a_is, g_is, x_is, and ρ_is are independent of each other.

The image formation is then modeled by

$$I(\mathbf{x}) = \sum_i^n a_i \, g_i\left(\frac{\mathbf{x} - \mathbf{x}_i}{\rho_i}\right). \qquad (15)$$

Each object with generator $g_i(\mathbf{x})$ in the scene contributes to the pixel value $I(\mathbf{x})$ according to $a_i g_i(\frac{1}{\rho_i}(\mathbf{x} - \mathbf{x}_i))$. Here, $\mathbf{x}$ is the pixel location in $\mathcal{T} \equiv [0, L] \times [0, L]$, $g_i : \mathcal{T} \mapsto \mathbb{R}^+$ is a generator of a randomly chosen object, $\rho_i \in [0, L]$ is a random scale, and a_i is a random weight associated with g_i. In short, it consists of the random linear combination of n randomly weighted random profiles.

This model aims at deriving probability models on an image by implicitly incorporating the variability of its ingredients. In this approach, Srivastava et al. [52] focus on the distribution of the gradient image $\partial I/\partial x$ or of filtered images $I^{(j)}(\mathbf{x}) = F^{(j)} * I(\mathbf{x})$, where $F^{(j)}$ is some band pass filter (for example, a Gabor filter). Under some assumptions, explicit computations in [13] lead to an analytic expression of the distribution function of the gradient image, namely *Bessel K forms*. Multidimensional distributions can also be explicitly derived. These results are extended to the filtered intensity $I^{(j)}$ in [52]. The interest of Bessel K forms is illustrated by their simple dependence on two parameters (p, c) that can be fitted to different images. They can be used for clutter classification, target recognition, and texture synthesis.

Despite their original rooting in different motivations, TGM (additive models) and CPC (multiplicative models) share many common features. Let us compare (15) to (14). Applied to some filtered image $I^{(j)}$ in place of $\log I(\mathbf{x})$, the

TGM above strikingly resembles the logarithm $\log Q_\ell(\mathbf{x})$ of some special CPC with log-normal multipliers W_i (then, $\log W_i \equiv a_i$ are i.i.d. normal variables) and a uniform distribution for $r_i \equiv \rho_i$ in place of the usual $1/r^3$—see (9)—and a random kernel (generator) $f(\mathbf{x}) \equiv g_i(\mathbf{x})$. Recall that we usually identify the intensity I to Q_ℓ and its logarithm $\log I$ to $\log Q_\ell$. Therefore, a fundamental difference between TGM and CPC lies in the quantity to be modeled: TGMs deal with *gradient images* $\partial I/\partial x$ or filtered images $I^{(j)}$, whereas CPCs deal directly with $\log I$ and I.

For both models, TGM and CPC, marginal distributions cannot be derived analytically in the most general case because of the nonconstant terms $g_i(\mathbf{x})$ or $f(\mathbf{x})$ (see Section 2.2.3). This is the reason why Grenander and Srivastava [13] proposed an empirical model using a GSM of scaled Γ densities, which led them to the family of Bessel K forms, which are (again!) infinitely divisible (but not compound Poisson). As a consequence, gradient images with Bessel K form statistics may be built, at least theoretically (see Section 2.1.2). However, their exact numerical synthesis may result to be difficult since they do not enter the family of CPCs. Most importantly, such synthetic images would be self-similar. Contrary to IDC, note that self-similarity was not explicitly taken into account in the construction of the TGM. Using IDC, one can build self-similar images associated to any Bessel K form, at least as a theoretical object. In addition to Bessel K form marginal distributions, such IDC gradient images would display the usual statistical properties of natural images, for example, a power law spectrum and power law correlations with prescribed exponents.

Interestingly, a remark in [52] on the link between the generator g and the Bessel K form parameters (p, c) might be of interest for IDC as well. Srivastava et al. note that p is small when g has sharp distinct boundaries and becomes greater as the frequency of occurrence (the intensity of the Poisson point process) increases. Given the similarity between TGMs and CPCs, this remark transposes to give instructive indications on how to choose the kernel f in (8) to tune the parameter p.

Finally, in [13], Grenander and Srivastava give a list of possible generalizations of their approach to get some desirable properties like inhomogeneity in space, local anisotropy, control on the regularity and smoothness of an image, prescribed departures from Gaussianity, and so forth. We emphasize that most of these generalizations can be obtained with IDC. IDC may account for *inhomogeneity in space* in at least two ways. One may play on the dependence of $dM(\mathbf{x}, r)$ on $\mathbf{x}$ either through the functional form of the control measure $dm(\mathbf{x}, r)$ or using a resolution $\ell(\mathbf{x})$ depending on the position $\mathbf{x}$. One may also change the kernel $f(\mathbf{x})$ from place to place, even at random as in the TGM. Models of random cascades on discrete trees [56], [60], [61] cannot play with inhomogeneity at will with the same versatility. These tree-based constructions suffer from the constraints imposed by the underlying discrete tree: only places corresponding to leaves of the tree (dyadic intervals) can be modified. Some *local anisotropy* may be introduced, thanks to the geometry of the kernel $f(\mathbf{x})$: this function acts like a shape parameter. Its support may not be a disk as for a cylindrical pulse and may display some anisotropy and dissymmetry (for example, an ellipse, a square, a star, a random shape, and so forth). The *regularity* and *smoothness* of the resulting image can be controlled as well. To this respect, the choice of the kernel function results crucial since its regularity determines (through a nonlinear process) the fine scale regularity of the image $I \equiv Q_\ell$. Last, almost any *departure from Gaussian distribution* can be obtained since the W_i can be any non-Gaussian suitable variable: heavy tailed distributions yield more "intermittent" images. As a conclusion, the numerous degrees of freedom of IDC may permit to suit a large variety of sets of images (countryside, urban zone, indoor scenes, and so forth), see Section 5 as well.

3.4 IDC and the Fokker-Planck Equation

The scale invariance property of natural images is linked to the absence of any characteristic scale in vision. The finer visible details of an image depend on the resolution at which the scene is observed. The sensor involves the sieving or box averaging of the scene at some limiting pixel size. Moreover, a large class of images is fractal [62]. Hence, more and more details appear when zooming in. This section aims at proposing a model to describe the influence of this finer scale of observation, the resolution, thanks to the link between IDC and a Fokker-Planck equation. This link was originally pointed out in [25] and [63] to describe the scale dependence of the statistics of a turbulent velocity field. It was also used in [64] to describe the intermittency phenomenon in turbulent flows. Our purpose is to adapt such ideas to natural images.

For a given visual sensor, details are lost due to an increase in the distance of observation or, equivalently, to a decrease in resolution that results in an averaging process (for example, textured regions become uniform regions). At infinitely large resolution $r \to +\infty$, a logarithmic sensor would see a limiting image with uniform average log-intensity $\log I_o$; then, the distribution is $P_\infty(\log I) = \delta_{\log I_o}(\log I)$. At the intermediate resolution $r = 1$ (scale 1 may correspond to the length of correlation in the image), correlations and fine details may be lost and only the large-scale variability described by some distribution P_1 remains. At an infinitely small resolution $r \to 0$, as the sensor gets closer to the scene, more and more details appear, and one expects that distributions become more and more leptokurtic (heavy tailed). This is much like a diffusion process where time would be replaced by the scale parameter $n(r) = \log(1/r)$. In particular, $r = 1$ corresponds to the "initial condition" at $n(r = 1) = 0$. As r tends to the $+\infty$, $n(r)$ goes to the $-\infty$: details are averaged together, and P_r concentrates onto a Dirac centered on the averaged log-intensity $\log I_o$ of the class of images to be modeled. As r goes to 0, $n(r)$ tends to ∞: more and more details arise, still respecting the fundamental self-similarity property and power law scaling.

One may want to model this phenomenon *for each image* by a diffusion equation on $I(\mathbf{x}, r)$, where the *time* is replaced by a *scale* parameter r, as in [65]. We rather propose to model *a class of images* by modeling the evolution of the distributions P_r of $Y = \log I_r$, where I_r is the intensity of the image observed at resolution r (the conditions which ensures that I_r is a well-defined random variable rely on the theory of martingales [28], [31], [46]). I_r may be seen as a low-pass filtered version (for example, $I_r \equiv \varepsilon_r$, see Section 2.2.3) of a limiting image with infinitely small resolution. To describe this evolution, we use the natural link between IDCs and Fokker-Planck equation that we recall below.

For simplicity, let us first consider the case of a Gaussian cascade for which $\tau(q) = -C_1 q + \frac{C_2}{2} q^2$ in (10). Then, rewriting scaling property (10), we get that $P_r(Y = \log I_r)$ has the following moment generating function $\tilde{P}_r(q) = \mathbb{E}[e^{qY}]$

$$\begin{aligned}\tilde{P}_r(q) &= e^{-\tau(q)\, n(r)} \cdot \tilde{P}_1(q) \\ &= \exp\left[\left(C_1 q + \frac{C_2}{2} q^2 \right) \cdot n(r) \right] \cdot \tilde{P}_1(q)\end{aligned} \tag{16}$$

where the C_k are the cumulants of G in (8). For a self-similar IDC obeying a power law scaling behavior as in (10), one has $n(r) = -\log r$ $(n(1) = 0,\ n(r) \to +\infty$ as $r \to 0)$. Deriving with respect to $n(r)$ and using the correspondence between successive powers of q in the development of $\tau(q) = -C_1 q + \frac{C_2}{2} q^2$ and the derivatives in the operator $\mathcal{U} = -C_1 \frac{\partial}{\partial Y} + \frac{C_2}{2} \frac{\partial^2}{\partial Y^2}$, we get

$$\frac{\partial \tilde{P}_r}{\partial n} = \left(C_1 q + \frac{C_2}{2} q^2 \right) \tilde{P}_r(q), \tag{17}$$

$$\Downarrow \quad \frac{\partial}{\partial Y} \equiv -q,$$

$$\begin{cases} \frac{\partial P_r}{\partial n} &= -C_1 \frac{\partial P_r}{\partial Y} + \frac{C_2}{2} \frac{\partial^2 P_r}{\partial Y^2} \\ P_{r=1} &= P_1 \quad (n(1) = 0). \end{cases} \tag{18}$$

Therefore, P_r obeys a Fokker-Planck equation. This argument extends to other infinitely divisible distributions, thanks to the theory of semigroups [25], [45], and (18) takes the general form ([45, Remark, p. 296])

$$\frac{\partial P_r}{\partial n} = \mathcal{U} P_r, \tag{19}$$

where $\mathcal{U}$ is the operator that describes the evolution of P_r with r. For compound Poisson distributions, the Fokker-Planck equation becomes

$$\frac{\partial P_r}{\partial n} = -(1 - \mathbb{E}W) \frac{\partial P_r}{\partial Y} - c P_r + c F * P_r, \tag{20}$$

where F is the distribution of $\log W$. Note that the self-similarity of images betrays a scale dilation invariant behavior, which is equivalent to a $\log$-scale translation invariance. Let us remark that, at resolution $r = 1$, the intensity of each pixel is the sum of the underlying details down to infinitely small scale $(\ell \to 0)$. In general, the distribution P_1 cannot be determined explicitly; one may simply expect that P_1 be close to a Gaussian due to a "Central Limit Theorem" effect (that is, at $r = 1$, the image would be modeled by Gaussian white noise). The evolution of distribution P_r is then governed in (19) from quasi-Gaussian P_1 to far from Gaussian (P_0).

Such a model using a Fokker-Planck equation describes the transition of distributions from the limiting "badly resolved" to the limiting "infinitely well resolved" image as a diffusion process. It explicitly takes into account the statistical self-similarity property of natural images. Such an approach might be extended to a family of band pass filtered versions of an image (for example, the $I^{(j)}$ in [52]) or to wavelet coefficients [25], [66].

3.5 IDC and Gaussian Scale Mixtures

We already noted in Section 3.2 that the Bessel-K forms proposed by Grenander and Srivastava [13] are indeed GSMs of scaled Γ densities. The theoretical development of the previous section leads us to further study the link between IDC and GSMs [55], [56]. It is easily seen that (16) actually accounts for the evolution of the pdfs of $Y_r = \log \varepsilon_r$ from a large scale r_1 to a smaller one r_2 through the equivalent convolution operation

$$P_{r_2} = G^{*\Delta n(r_1, r_2)} * P_{r_1}, \tag{21}$$

where G is an infinitely divisible distribution with a moment generating function $\tilde{G}(q) \propto e^{-\tau(q)}$. Thus, the relationship between scales r_1 and r_2 is described by the so-called propagator $G_{r_1, r_2} = G^{*\Delta n(r_1, r_2)}$, where G is called the "kernel," and $\Delta n(r_1, r_2)$ is the "number of steps" of the cascade from r_1 to r_2. Reading G_{r_1, r_2} as the distribution of a random variable $\tilde{\omega}_{r_1, r_2} = \log W_{r_1, r_2}$ independent of $Y_{r_1} = \log \varepsilon_{r_1}$ and $Y_{r_2} = \log \varepsilon_{r_2}$, we get

$$\varepsilon_{r_2}(\mathbf{x}_2) \stackrel{d}{=} W_{r_1, r_2}(\mathbf{x}_1, \mathbf{x}_2) \cdot \varepsilon_{r_1}(\mathbf{x}_1), \tag{22}$$

where $\stackrel{d}{=}$ stands for equality of distributions. Thus, ε_{r_2} can be expressed as the product of ε_{r_1} and an independent positive scalar random variable W_{r_1, r_2}, the *multiplier*. This is precisely the structure of a general scale mixture for a given distribution of ε_{r_1} at some reference scale r_1 (for instance, one may choose $r_1 = 1$). It reduces to a GSM if ε_{r_1} is a zero-mean Gaussian variable.

Equations (21) and (22) extend to wavelet coefficients [26], [27], [37], [38], [49], [67] in place of ε_r. Then, a GSM may appear since it is usually expected that wavelet coefficients have Gaussian statistics at large scales. IDCs are therefore consistent with the modeling of natural images by GSMs as proposed by some authors [2], [3], [55], [56]. We emphasize that the complete description of an IDC is formally equivalent to the complete description of the correlation structure of those hidden random multipliers $W_{r_1, r_2}(\mathbf{x}_1, \mathbf{x}_2)$ evoked above, for any $(\mathbf{x}_1, r_1)$ and $(\mathbf{x}_2, r_2)$, recall Section 3.6.

As far as the simulation of some given image is concerned, (21) tells us that matching wavelet coefficients marginals at all scales is a minimum condition to achieve; but this is not sufficient. For instance, Field [12] proposed to use i.i.d. random variables to simulate wavelet coefficients independently at each scale. Such an approach prescribes no multiscale correlations but only second-order time correlations (that is, the spectrum). Heeger and Bergen [68] have proposed an iterative scheme to match both pixel values histograms and steerable pyramid coefficients (or wavelet coefficients) histograms. We see this scheme as an implicit numerical method to solve (21). Moreover, by imposing the consistency between local information (pixel values) and multiscale properties (steerable pyramid), this scheme imposes some multiscale correlation structure. Wei and Levoy [69] and Gallagher and Kokaram [70] have also proposed multiscale methods for texture synthesis that try to implicitly learn the local structure of a texture at various resolutions. Wainwright et al. [55], [56] have proposed to use GSMs based on an underlying multiplicative cascade (with hidden multipliers) on wavelet coefficients. Thus, interestingly, not only marginals and second-order correlations are imposed, but multiscale correlations at higher orders are controlled as well. This latter approach sounds closely connected to the random wavelet cascades proposed by Arneodo et al. [71] in turbulence.

3.6 Multivariate Statistics

In addition to non-Gaussian behavior of marginal statistics, IDC have nontrivial multivariate statistics. Fig. 5 shows the joint and conditional histograms of the wavelet coefficients of an IDC. These observations are quite similar to those by Wainwright and Simoncelli (see Fig. 4 in [55] or Fig. 1 in [2]). These results can also be compared to the irregular polyhedralike shapes found by Lee et al. [57] in contour surfaces of histograms of occlusion models. Such properties

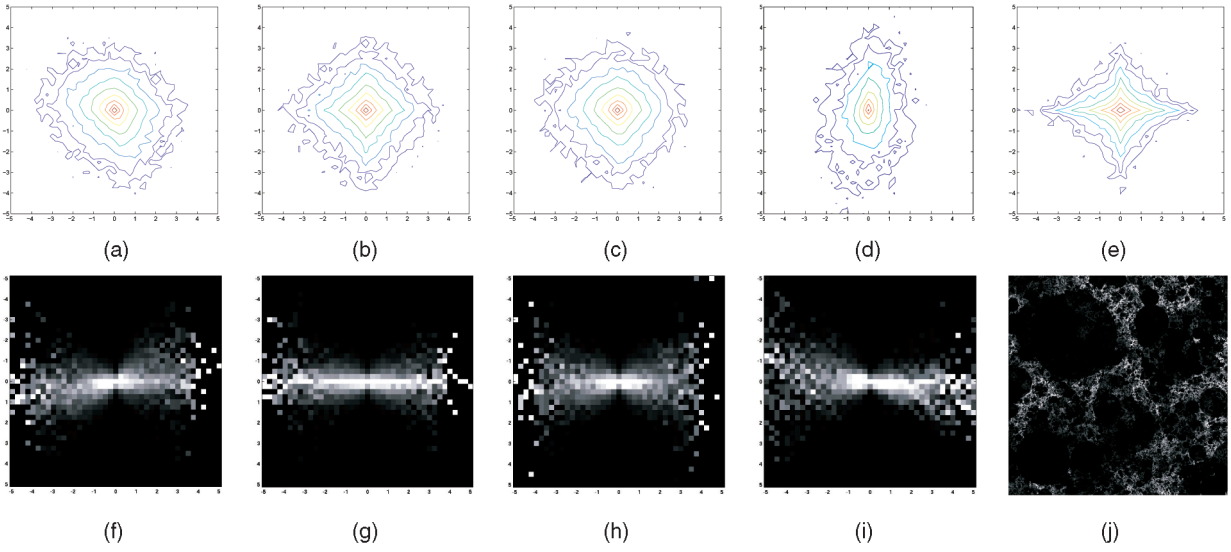

Fig. 5. Bivariate histograms of the wavelet coefficients associated with different basis functions for one single CPC image (compare to Wainwright and Simoncelli [55]). Top row shows contour plots of log probability. (a) and (b) are for different spatial offsets (same scale and orientation), (c) is for different orientations (same scale and nearly same position), (d) corresponds to a pair at adjacent scales (same orientation and nearly same position), (e) is for remote neighbors at large spatial offset. Bottom row shows some conditional distributions: brightness corresponds to larger frequency, and (j) is the CPC image itself.

are usually linked to the occurrence of simple geometries in images with partially constant intensity regions and sharp discontinuities.

We emphasize that such observations are consistent with an underlying multiplicative cascade. Let us assume that we are studying two random variables X_1 and X_2 (for example, two wavelet coefficients at different positions, scales, or orientation). Moreover, let us assume that there exists some random variable z independent of X_1 and X_2 such that $X_2 \overset{d}{=} z \cdot X_1$. Denoting by p_z the pdf of z, one has, for the conditional pdf, $p(X_2|X_1) = p(zX_1|X_1) = \frac{1}{|X_1|} p_z(z) = \frac{1}{|X_1|} p_z(\frac{X_2}{X_1})$. Therefore, one expects that the width of $p(X_2|X_1)$ increases linearly with $|X_1|$, which yields this characteristic butterfly pattern on the bottom row of Figs. 5f, 5g, 5h, and 5i.

3.7 Bessel I Forms

This section reports on a particular family of compound Poisson distributions, which we propose to call *Bessel I forms*, in analogy with Bessel K forms. Bessel I forms appear as a family of simple compound Poisson models depending on one parameter only. Their numerical synthesis is simple and theoretical computations can be carried out explicitly. Moreover, an equivalent model was previously introduced by Castaing [66], and Chainais [1], [25] to model the distributions of velocity increments measured in a turbulent fluid flow. These models may be relevant to describe the statistics of natural images as well.

The main ingredients of the construction of Bessel I forms are the following. Let $\underline{F}$ (respectively, F) denote the pdf of the multipliers W (respectively, $\omega = \log W$) of a CPC as defined in (6) with a cylindrical kernel $f = \mathbb{1}_{\mathcal{D}_{1/2}}$. As a particular case of interest, we consider the choice

$$\begin{aligned} &F(\omega) = \lambda e^{\lambda\omega}, \quad \omega \in (-\infty, 0], \\ \Leftrightarrow\ &\underline{F}(W) = \lambda W^{\lambda-1}, \quad \lambda > 0,\ W \in [0,1]. \end{aligned} \tag{23}$$

The case $\lambda = 1$ corresponds to uniformly distributed variables W in [0, 1]. For a scale invariant CPC with $m(\mathcal{C}_\ell) = c \log(1/\ell)$ $(c > 0)$, the distribution $G_\ell(Y)$ of $Y = \log Q_\ell \equiv \log I$ takes the following explicit form:

$$G_\ell(Y) = \ell^c \sum_{k=0}^{\infty} \frac{(c \log(1/\ell))^k}{k!} F^{*k}(Y - (1 - \mathbb{E}W)), \tag{24}$$

where F^{*k} is the kth convolution of F. After some computations, one gets a distribution $G_\ell(Y)$ with an atom ℓ^c at the origin and described for $Y < 0$ by

$$G_\ell(Y) = \ell^c \sum_{k=1}^{\infty} \frac{(c\lambda \log(1/\ell))^k |Y|^{k-1}}{k!(k-1)! e^{-\lambda|Y|}},$$

$$G_\ell(Y) = \ell^c \sqrt{\lambda c \log(1/\ell)} \frac{e^{-\lambda|Y|}}{\sqrt{|Y|}} I_1(2\sqrt{\lambda c \log(1/\ell)|Y|}), \tag{25}$$

where I_1 is the modified Bessel function of the first kind of order 1 [45]. This distribution G_ℓ in (25) is infinitely divisible since it is a compound Poisson distribution. In the context of natural images, we propose to call them *Bessel I forms* in reference to Bessel K forms. The corresponding scaling exponents are given by

$$\tau(q) = \varphi(q) = \frac{cq(q-1)}{(\lambda+1)(q+\lambda)}. \tag{26}$$

In the work by Castaing [66], the parameter $\lambda \equiv 1/T$ is interpreted as the inverse of a "temperature" T of a turbulent flow. For $\lambda \ll 1$ (high temperature $T \gg 1$), $\underline{F}(W)$ concentrates around 0 (see (23)). One expects to observe dark images with a lot of black regions associated to small values of $Q_\ell \equiv I$ and some isolated white points associated to rare extreme values of I. For $\lambda \gg 1$ (low temperature $T \ll 1$), $\underline{F}(W)$ concentrates around 1, and the $e^{-\lambda|Y|}$ term in (25) is rapidly decreasing as $Y \to -\infty$: one expects to observe rather homogeneous

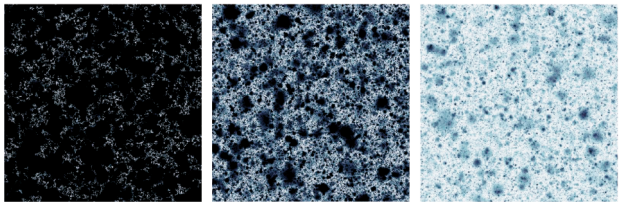

Fig. 6. Examples of a CPC associated to Bessel I forms with parameters (a), (b), and (c) $\lambda = 0.1$, 1.0, and 10, respectively.

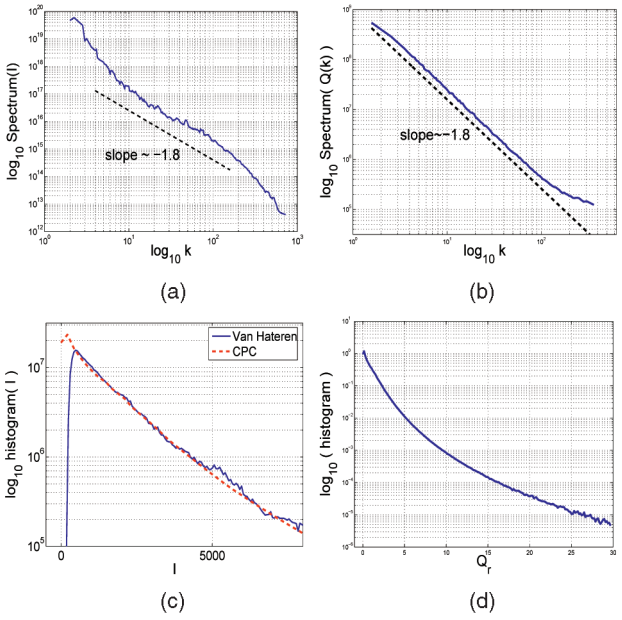

Fig. 7. (a) and (b) Averaged spectrum of intensity of 400 images from van Hateren data basis [5] compared to CPC images. (c) and (d) Averaged histograms of the intensity of 400 van Hateren and CPC images, respectively.

images with few isolated small values—compare Figs. 6a, 6b, and 6c. In fact, the effect of λ is combined with the effect of the resolution ℓ in the product $\lambda c \log(1/\ell)$. The smaller the resolution $0 < \ell < 1$, the deeper the cascade. The quantity $c \log(1/\ell)$ is a measure of the clutter in the image so that the bigger $c \log(1/\ell)$, the heavier the tails of the distribution. Therefore, one may tune both parameters λ and $c \log(1/\ell)$ to model a large class of empirical log-intensity distributions. We emphasize that images associated to Bessel I forms can be easily synthesized numerically—see Fig. 6.

4 Experiment

This section aims at demonstrating that IDC images obey most of the statistical properties usually observed on natural images. To this purpose, we systematically carry out the statistical analysis of a set of 400 simulated IDC images and compare it to the analysis of a set of 400 images from the van Hateren database [5]. We show that IDCs clearly obey nontrivial properties of natural images so that we can state that IDCs are a very good candidate to model natural images.

4.1 Intensity Is Scale Invariant and Non-Gaussian

Fig. 7a shows the average power spectrum of the intensity I of a set of 400 images from the van Hateren data basis [5]. The estimated slope is about -1.8, which is consistent with other

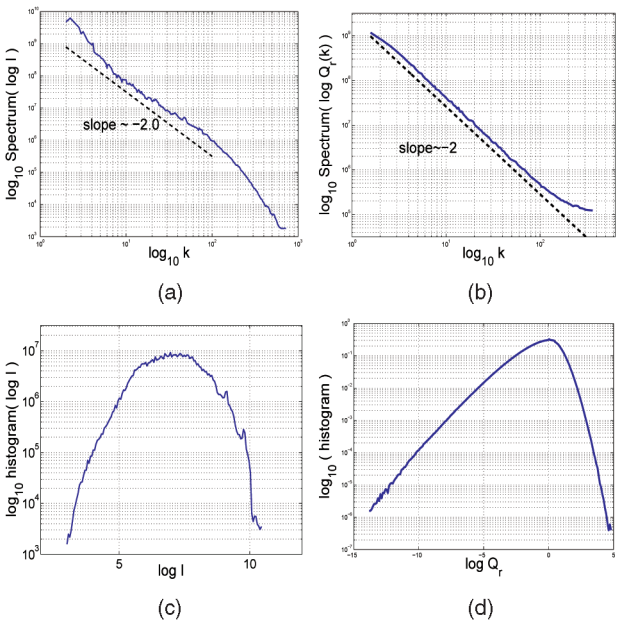

Fig. 8. (a) and (b) Averaged Fourier spectrum (squared amplitude of the Fourier components) of log-intensity of 400 images from van Hateren data basis [5] compared to 400 CPC images. (c) and (d) Averaged histograms of log-intensity of 400 van Hateren and CPC images, respectively.

estimates reported in the literature [2], [3], [9], [10]. For images simulated using IDC, the spectrum is $\propto 1/k^{2+\tau(2)}$. By choosing some adequate distribution of the multipliers W_i of CPCs, we set $\tau(2) \simeq -0.2$, which yields a spectrum $\propto 1/k^{1.8}$ (see Section 2.2), as can be checked in Fig. 7b.

The histograms of intensity I of the 400 Van Hateren and CPC images are shown in Figs. 7c and 7d. Although no parameter has been adjusted here, a similar functional shape is observed with a slow decrease in the log-log plot. Intensity is clearly non-Gaussian in both cases. The histogram has a maximum that is close to zero and displays a slow decrease toward high values.

4.2 Log-Intensity Is Scale Invariant and Non-Gaussian

Fig. 8a shows a power spectrum estimated from the contrast $\log I$ on a set of 400 images from the van Hateren data basis [5]. The estimated slope is about -2, which is consistent with other estimates reported in the literature [2], [9], [10]. For images simulated using CPC, the spectrum has a $\propto 1/k^2$ behavior as well, see Fig. 8b.

The histograms of $\log I$ for the 400 van Hateren and CPC images are shown in Figs. 8c and 8d. No parameter has been adjusted here. The similarity between both histograms is rather approximate and essentially limited to a strong skewness to the left. The log-intensity is clearly non-Gaussian in both cases. Note that such a histogram is difficult to estimate precisely on images from the van Hateren data basis due to a lack of quantification (limited to 12 bits).

4.3 Coarse-Grained Intensity Obeys Multifractal Scaling

Fig. 9 shows the results of the multifractal analysis of the images from the van Hateren database. Fig. 9a checks for the relevance of such an analysis. A clear scaling behavior of the

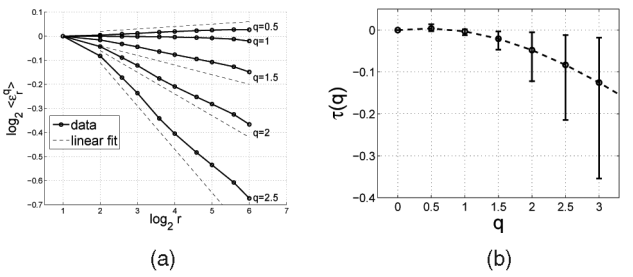

Fig. 9. Multifractal analysis of a set of 400 images from the van Hateren database. (a) Observation of the behavior $\mathbb{E}\varepsilon_{\mathbf{r}}^{q} \propto \mathbf{r}^{\tau(q)}$ over nearly five octaves for one individual image. (b) The averaged observed exponent $\tau(q)$ display a nonlinear behavior; error bars correspond to the empirical 95 percent confidence intervals.

form (see (10)) $\mathbb{E}[\varepsilon_r^q] \sim r^{\tau(q)}$ $(0 \leq q \leq 3)$ is observed on individual images. The empirical 95 percent confidence intervals show that the exponents $\tau(q)$ estimated from the set of images significantly depart from a linear behavior, see Fig. 9b. As a consequence, a multifractal approach is relevant. Recall that IDCs were originally designed to obey statistical properties observed on signals probed in turbulent fluid flows (cf. the multifractal formalism). Here, we see that they share higher order statistical properties with natural images as well.

Note that we do not pretend that each image is multifractal in any region, but only that, on the average, a multifractal model like IDC may be relevant when dealing with the statistical properties of a large set of natural images. Natural images combine various kind of singularities due to the presence of edges, where strong variations occur, and textured regions (that may be multifractal themselves).

4.4 Correlations of I and $\log I$

Another quantity to look at is the correlation of the intensity $C_I(\mathbf{x}) = \mathbb{E}[I(0)I(\mathbf{x})]$, respectively, of the contrast (log-intensity) $C_{\log I}(\mathbf{x}) = \mathbb{E}[\log I(0) \log I(\mathbf{x})]$—see Fig. 10. According to Mumford and Gidas [10], as a consequence of the scale invariance property, a relevant model should display a power law correlation function for the intensity. Figs. 10a and 10b shows this behavior for the set of 400 images from the van Hateren data basis. This is also a classical property of multiplicative cascades. For IDC, these correlations are known to be, respectively, $C_I(\mathbf{x}) \propto |\mathbf{x}|^{\tau(2)}$ and $C_{\log I}(\mathbf{x}) \propto \log|\mathbf{x}|$—see Figs. 10c and 10d. We emphasize that such nontrivial properties are consistent with the results on power spectrum densities even though it is more difficult to check. Note that the apparent variance in Figs. 10a and 10b is due to the averaging over all directions. A much smoother curve (suggesting less variance) would be observed for the horizontal or vertical correlations only for instance. Despite a larger correlation length in the horizontal direction than in the vertical one, the qualitative behavior remains the same for all directions for $\|\mathbf{x}\| \leq 64$ pixels.

4.5 IDC versus Ruderman and Bialek's Analysis

In [4], [8], [9], Ruderman and Bialek report on the statistical analysis of a set of 54 images taken in the woods of Hacklebarney State Park in central New Jersey. They study the link between non-Gaussian distributions and the inhomogeneity of gradients by defining the coarse-grained log-contrast $\phi_N(\mathbf{x})$ of $\phi = \log(I/I_o)$ in an $N \times N$ block

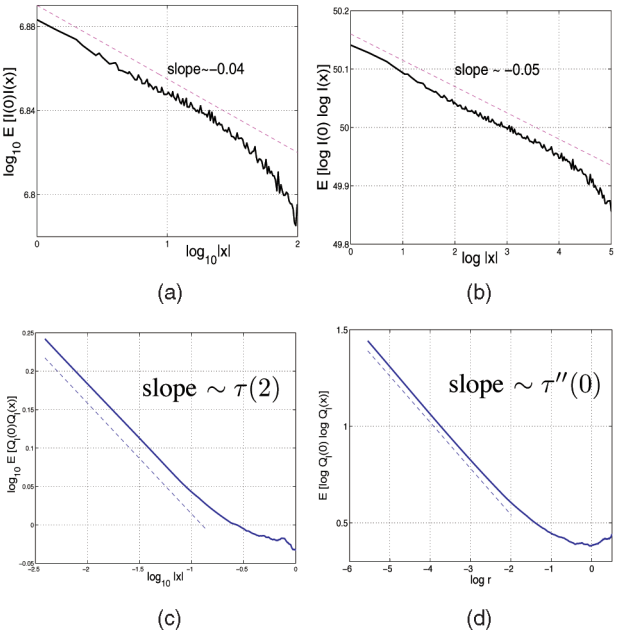

Fig. 10. (a) and (b) Correlation functions for I and $\log I$ estimated from a set a 400 natural images from van Hateren database. One observes that $\mathbb{E}[\mathbf{I}(\mathbf{0})\mathbf{I}(\mathbf{x})] \propto |\mathbf{x}|^{\alpha}$ and $\mathbb{E}[\log \mathbf{I}(\mathbf{0}) \log \mathbf{I}(\mathbf{x})] \propto \log|\mathbf{x}|$. (c) and (d) For CPC, $\mathbb{E}[\mathbf{Q}_\ell(\mathbf{0})\mathbf{Q}_\ell(\mathbf{x})] \propto |\mathbf{x}|^{\tau(\mathbf{2})}$ over nearly two decades: The observed slope exponent is prescribed by the choice of $\varphi(2)$; $\mathbb{E}[\log \mathbf{Q}_\ell(\mathbf{0}) \log \mathbf{Q}_\ell(\mathbf{x})] \propto \log|\mathbf{x}|$ betrays a multiplicative correlation structure.

surrounding each point $\mathbf{x}$. Denote by σ_N the variance of $\phi_N(\mathbf{x})$ for fixed N. Then, the normalized quantities $\phi_N(\mathbf{x})/\sigma_N$ are found to be close to identically distributed. We show below that this is again consistent with the IDC approach. Let ω be a random variable distributed by the common (zero mean and unit variance) distribution of the $\phi_N(\mathbf{x})/\sigma_N$, and let $W = e^{\omega}$. Denote by $I_N(\mathbf{x}) = \exp[\phi_N(\mathbf{x})]$. Using our notations, the result in [4], [9] can be rewritten as

$$\begin{aligned} \frac{\phi_N(\mathbf{x})}{\sigma_N} \overset{\text{in law}}{=} \omega \Leftrightarrow \phi_N(\mathbf{x}) \overset{\text{in law}}{=} \omega \cdot \sigma_N \\ \Rightarrow I_N(\mathbf{x}) \overset{\text{in law}}{=} W^{\sigma_N}. \end{aligned} \tag{27}$$

Thus, a multiplicative hierarchy appears (in law) as the (geometrically) averaged intensity $I_N(\mathbf{x})$ over $N \times N$ pixels is concerned. This gives some precise sense to the "hidden multipliers" evoked in [2], which sound much like the Novikov's "breakdown coefficients" in turbulence [72]. This observation advocates once more for the interest of the IDC framework. The quantity σ_N then appears as a measure of the clutter at scale N that can be interpreted as the depth of a multiplicative cascade—see Section 3.1. As already mentioned in Section 3.5, the results by Wainwright and Simoncelli [55], [56] based on the GSM model also advocate for this hidden multiplier structure by studying the local variance.

Such a "self-similarity" of the log-contrast histograms is expected on IDC images with $\sigma_N \propto \tau(2) \log N$. Fig. 11 shows numerical results obtained from several independent realizations of 512×512 images generated using an IDC. Rescaled histograms have very similar shapes, Fig. 11b. Let us recall that Ruderman [4] expected a power law dependence of the form $\sigma_N \propto N^{-\nu}$. Therefore, linear regressions in the log-log plots of σ_N versus N gave $\nu \simeq -0.2$ (which is a small exponent) as a rough estimate on

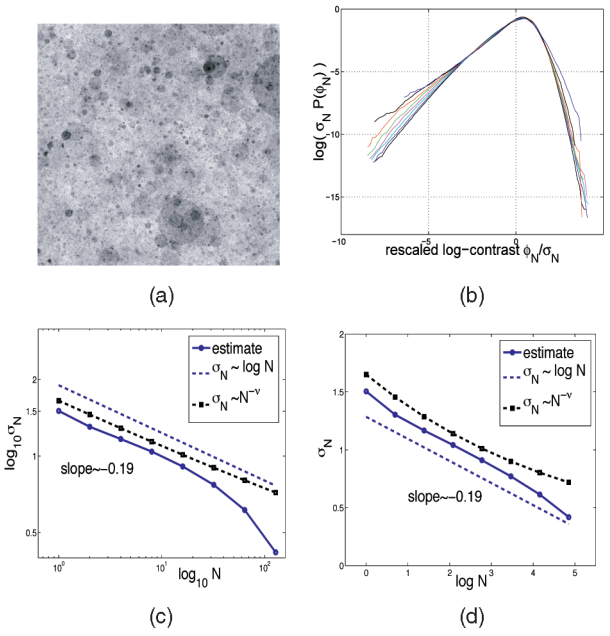

Fig. 11. (a) Example of a realization of a CPC with the same parameters as for all other figures, and (b) illustration of the self-similarity of coarse-grained log-contrast histograms over scales $N = 2^j$ for $0 \leq j \leq 7$ (from $N = 1$ to 128). (c) Log-log plot of the standard deviation σ_N of ϕ_N distribution as a function of N; (d) log-linear plot of the standard deviation σ_N of ϕ_N distribution as a function of N.

images taken in the woods, Fig. 11c. However, a log-log plot often hides many details: both the $N^{-\nu}$ model and the $A - B \log N$ model fit the data equally well in a log-log plot. When modeling images as IDCs, we are rather led to propose a model of the form $\sigma_N \simeq A - B \log N$, see Fig. 11d where a log-linear plot is shown. Here is one more evidence of the relevance of IDC for the modeling of natural images even though further study would be needed to discriminate between these models. This might be of importance when optimizing some denoising method for instance.

5 Procedural Texture Synthesis

5.1 Some Possibilities

Eventually, we want to put the emphasis on the potential use of IDC in two dimensions for procedural texture synthesis. We mentioned above the many degrees of freedom of IDCs, for example, in Section 3.2. Scaling exponents can be prescribed, the scaling range can be precisely defined, there is no preferred scale ratio as in discrete constructions so that properties are observed over a continuum in space and scale, a wide class of non-Gaussian models are available, geometrical features (for example, anisotropy) can be taken into account, and so forth. Playing with the control measure $dm(\mathbf{x}, r)$, the distribution of multipliers $\underline{F}(W)$, the local resolution $\ell(\mathbf{x})$, the regularity and geometry of the kernel $f(\mathbf{x})$, and so forth, one may obtain a wide variety of textures. Once more, we point to the easy implementation of CPC as well. Several examples are presented in Fig. 12.

Most texture synthesis methods actually use an additive approach relying on the use of some functional basis like wavelets [56], [70], [73] or morphlets [60]. Then, many simple actions like zooming in or locally modifying any region of an image are difficult mainly because of the use of a discrete

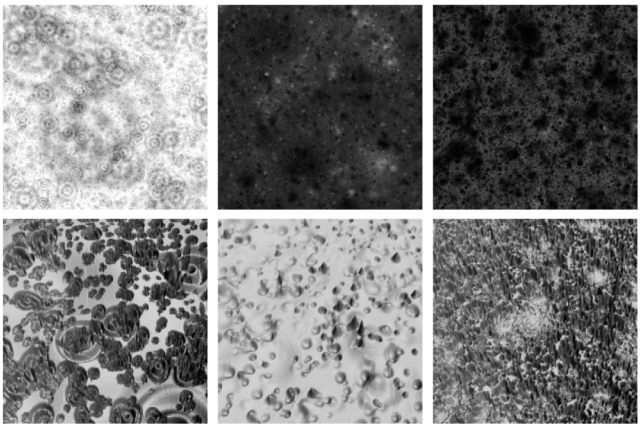

Fig. 12. Examples of textures obtained using CPC with different kernels: gray levels and 3D surface representations.

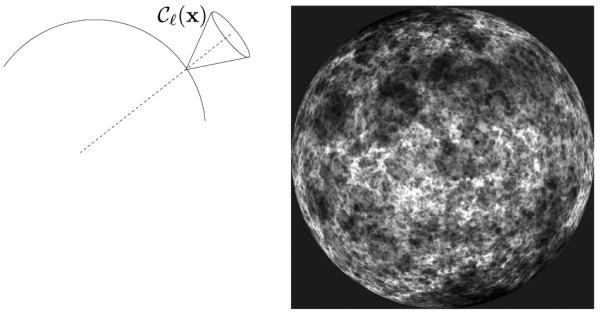

Fig. 13. Principle of the synthesis of a texture directly on a curved manifold using a CPC and an example of a texture directly generated on a sphere using a CP (gray levels)

tree-based construction. Some blocking effects may appear. CPCs avoid the blockiness of tree-based methods and permit to define the texture locally without any constraint on the geometry of the region of interest. Aliasing, zooming, inhomogeneity, anisotropy, and so forth can be controlled locally in a very easy manner. For instance, finer details could be progressively and dynamically generated as more and more small scales are needed. Moreover, CPCs permit to adapt the resolution locally to avoid aliasing artifacts. Furthermore, the integration kernel $f(\mathbf{x})$ in (6) plays a role similar to that of the wavelet in a random wavelet expansion, but it is not assigned to any deterministic position. Last, the choice of some basic pattern $f(\mathbf{x})$ results in some particular texture [74], see Fig. 12.

5.2 Textures on Manifolds

Another advantage of IDCs is that the synthesis of a CPC on a manifold results rather simple. It suffices to work with the cone $\mathcal{C}_\ell(\mathbf{x})$ around the normal to the manifold at position $\mathbf{x}$—see Fig. 13. Provided that the curvature of the manifold is not too large (radius $R \gg 1$), the algorithm generalizes naturally: 1) generate a random Poisson point process within a spherical corona $R < |\mathbf{x}| < R + 1$, 2) generate associated random multipliers W_i with given law $\underline{F}$, and 3) compute $Q_\ell(\mathbf{x})$ on the sphere of radius R using (6). This is a very interesting direction of work since it permits to avoid classical artifacts due to the classical mapping of a planar texture on a curved surface, for example, a sphere [74]. Fig. 13 shows the result of the direct synthesis of a CPC on a sphere: there is no pole nor equator artifact in contrast with what

happens with the usual texture mapping. Remarkably, even with no use of any perspective effect, the picture seems to be 3D, whereas it is only a 2D projection. Another possibility would be to synthesize and cut a 3D IDC texture with respect to the desired manifold to deduce the 2D texture on this manifold.

5.3 Software

Software and demos are available from our Web page. Note that IDCs in N dimensions may also result as useful to synthesize multifractal scalar fields (3D, (for example, turbulent dissipation field), dynamical textures ($3\mathrm{D} = 2\mathrm{D} + \mathrm{t}$, for example, moving texture), dynamical 3D scalar fields ($4\mathrm{D} = 3\mathrm{D} + \mathrm{t}$, for example, moving 3D cloud), and so forth). For instance, one can obtain a multifractal film as a series of multifractal pictures with multifractal time evolution. The film is obtained by taking each image as a 2D slice of a 3D scalar field generated using a CPC; the third dimension is used as a time parameter. Then, each image is a multifractal image; the time evolution of one particular pixel is multifractal as well. A sample of such a film can be downloaded from our Web site.

6 Conclusion

In summary, we have presented a new family of stochastic processes for the modeling of natural images, namely, IDCs. This family of multifractal processes was first designed to model scalar fields in turbulent fluid flows [1], [29], [30], [41]. From a theoretical point of view, IDCs are mathematically sound [1], [28], [31], [46]. Our purpose was to show that IDCs fulfill most of the desired properties a "good model" of natural images should have, including nontrivial multivariate statistics [2], [55], [57].

Notably, the IDC framework shares many properties with the work by Mumford and Gidas [10] where an axiomatic approach relying on the use of infinitely divisible distributions was proposed. However, there are important differences between IDCs and this former approach. Above all, IDCs belong to the family of multiplicative cascades, whereas Mumford and Gidas rather used a purely additive approach. We have shown that IDCs provide a way to describe the self-similar behavior of both the intensity I and its logarithm $\log I$ within a consistent framework. The clutter notion, as defined in [10], then receives a quantitative meaning as the depth $\log(1/\ell)$ of a multiplicative cascade. Among the full generality of the IDC framework, the CPCs are particularly attractive since they receive a rather intuitive physical interpretation, which can be compared to other works [13], [52], [53], [54], [59], where natural images are modeled by the projection of a random distribution of objects in space. In particular, we have focused on the TGMs and Bessel K forms proposed by Grenander and Srivastava in [13], [52]. We have shown that, under some conditions, the logarithm of a CPC and a TGM could be seen as similar models. These approaches give complementary insights to the modeling of natural images. Turning to the modeling of the distributions of multiscale quantities (for example, wavelet coefficients), we have shown an interesting correspondence between IDC models and some Fokker-Planck equation, which describes the dependence of their statistics on the scale of observation. We have shown that changing the scale of observation amounts to a forward or backward evolution of the probability densities (for example, of the wavelet coefficients) governed by this Fokker-Planck equation. This last remark has led us to shed some light on the deep connections between the IDCs and the GSMs proposed by Wainwright and Simoncelli [55], [56]. Both of them rely on the introduction of "hidden multipliers" to describe the correlation structure of an image. Referring to the infinitely divisible Bessel K forms proposed by Grenander and Srivastava [13] to model the gradient image intensity, we have introduced the Bessel I forms to directly model the intensity itself. We advocate for the use of Bessel I forms, which are special CPCs that depend on one parameter only, to model the intensity $I(\mathbf{x})$ of natural images. Bessel I forms can be easily synthesized numerically. They may be relevant to model pdfs of an image at different resolutions.

To make our claim even more convincing and concrete, we have analyzed a set of 400 images from the van Hateren database [5]. We have estimated histograms, spectra, correlation, and multifractal scaling properties both on the intensity $I(\mathbf{x})$ and on its logarithm $\log I$ (sometimes called the contrast). All our observations are consistent with the IDC framework. Even the "paradoxical" analogies between observations on I and $\log I$ can be consistently understood in this approach. Therefore, IDCs appear as a very rich theoretical framework as far as the modeling of natural images is concerned. They are consistent with the usual assumptions of most of the already known models, and they shed a new light on interconnections between various approaches.

Finally, we focused on the application of IDC to procedural texture synthesis. The large number of degrees of freedom of IDC and, above all, CPC (for example, scaling properties, local control of inhomogeneity, and anisotropy) makes them very easy to play with for aesthetic purpose. CPCs can even be synthesized directly on a manifold, for example, a sphere, while preserving all their statistical properties, with no mapping artifacts. Furthermore, 3D textures can also be obtained using IDCs, as well as $2\mathrm{D} + \mathrm{t}$ or $3\mathrm{D} + \mathrm{t}$ animated and dynamical textures. Software and examples can be downloaded from our Web page.

Some interesting research remains to be done around IDCs. One direction is the study and the optimization of image processing tools based on a Bayesian approach under the assumption that images belong to some class of IDC. We expect that efficient Bayesian methods might be elaborated using some IDC model, for instance, in the spirit of the work by Fadili and Boubchir [75] or even by adapting some ideas by Wainwright et al. [56]. An IDC-based image processing method would benefit from their ability to precisely model the statistical features of natural images and to locally take into account the geometrical properties of an image where preferential directions, edges, and varying textures play a central role. Another important direction is the application of IDC to the modeling of various physical systems like turbulent scalar fields, clouds, porous media, and so forth. This is the subject of ongoing work.

Part of the results presented in this paper were communicated to Groupe de recherche et d'études du traitement du signal et des images (GRETSI '05) [74] and to International Conference on Image Processing (ICIP '05) [34].

Acknowledgments

The author would like to thank P. Abry, V. Barra, J. Barral, S. Deguy, J.-J. Li, and R. Riedi for stimulating discussions.

REFERENCES

[1] P. Chainais, "Multidimensional Infinitely Divisible Cascades. Application to the Modelling of Intermittency in Turbulence," *European Physical J. B,* vol. 51, pp. 229-243, 2006, DOI: 10.1140/epjb/e2006-00213-y.

[2] A. Srivastava, A. Lee, E. Simoncelli, and S.-C. Zhu, "On Advances in Statistical Modeling of Natural Images," *J. Math. Imaging and Vision,* vol. 18, pp. 17-33, 2003.

[3] E. Simoncelli, "Statistical Modeling of Photographic Images," *Handbook of Video and Image Processing,* A. Bovik, ed. Academic Press, 2005.

[4] D. Ruderman, "The Statistics of Natural Images," *Network: Computation in Neural Systems,* vol. 5, pp. 517-548, 1994.

[5] J. van Hateren and A. van der Schaaf, "Independent Component Filters of Natural Images Compared with Simple Cells in Primary Visual Cortex," *Proc. Royal Soc. London Series B,* vol. 265, pp. 359-366, http://hlab.phys.rug.nl/archive.html, 1998.

[6] D. Field, "Relations between the Statistics of Natural Images and the Response Properties of Cortical Cells," *J. Optical Soc. Am. A,* vol. 12, pp. 2379-2394, 1987.

[7] N. Deruigin, "The Power Spectrum and the Correlation Function of the Television Signal," *Telecomm.,* vol. 1, no. 7, pp. 1-12, 1956.

[8] D. Ruderman, "Origins of Scaling in Natural Images," *Vision Research,* vol. 37, no. 23, pp. 3385-3398, 1997.

[9] D. Ruderman and W. Bialek, "Statistics of Natural Images: Scaling in the Woods," *Physical Rev. Letters,* vol. 73, no. 3, pp. 814-817, 1994.

[10] D. Mumford and B. Gidas, "Stochastic Models for Generic Images," *Quarterly of Applied Math.,* vol. LIV, no. 1, pp. 85-111, 2001.

[11] D. Field, "Scale Invariance and Self-Similar Wavelet Transforms: An Analysis of Natural Scenes and Mammalian Visual Systems," *Wavelets, Fractals and Fourier Transforms: New Developments and New Applications,* Oxford Univ. Press, 1993.

[12] D. Field, "What Is the Goal of Sensory Coding?" *Neural Computation,* vol. 6, pp. 559-561, 1994.

[13] U. Grenander and A. Srivastava, "Probability Models for Clutter in Natural Images," *IEEE Trans. Pattern Analysis and Machine Intelligence,* vol. 23, no. 4, pp. 424-429, Apr. 2001.

[14] J. Huang and D. Mumford, "Statistics of Natural Images and Models," *Proc. IEEE Conf. Computer Vision and Pattern Recognition,* pp. 541-547, 1999.

[15] A. Ayache, S. Léger, and M. Pontier, "Drap Brownien Fractionnaire," *Potential Analysis,* vol. 17, no. 31-43, 2002.

[16] H. Biermé, "Champs Aléatoires: Autosimilarité, Anisotropie et Étude Directionnelle," PhD dissertation, Orléans Univ., 2005.

[17] U. Frisch, *Turbulence. The Legacy of A. Kolmogorov.* Cambridge Univ. Press, 1995.

[18] U. Frisch and G. Parisi, "Fully Developed Turbulence and Intermittency," *Proc. Int'l Summer School on Turbulence and Predictability in Geophysical Fluid Dynamics and Climate Dynamics,* pp. 84-88, 1985.

[19] S. Jaffard, "Multifractal Formalism for Functions, Part 1 and 2," *SIAM J. Math. Analysis,* vol. 28, no. 4, pp. 944-998, 1997.

[20] R.H. Riedi, "Multifractal Processes," *Theory and Applications of Long Range Dependence,* Doukhan, Oppenheim, and Taqqu, eds., pp. 625-716. Birkhauser, 2003.

[21] A. Turiel, G. Mato, and N. Parga, "Self-Similarity Properties of Natural Images Resemble Those of Turbulent Flows," *Physical Rev. Letters,* vol. 80, no. 5, pp. 1098-1101, 1998.

[22] A. Turiel and N. Parga, "The Multifractal Structure of Contrast Changes in Natural Images: From Sharp Edges to Textures," *Neural Computation,* vol. 12, pp. 763-793, 2000.

[23] A. Arneodo, C. Baudet, R. Benzi, B. Castaing, R. Chavarria, S. Ciliberto, F. Chilla, B. Dubrulle, B. Hebral, J. Herweijer, J. Maurer, J.-F. Muzy, A. Noullez, J. Peinke, W. van de Water, and H. Willaime, "Structure Functions in Turbulence, in Various Flow Configurations, at Reynolds Number between 30 and 5000, Using Extended Self-Similarity," *Europhysics Letters,* vol. 34, no. 6, pp. 411-416, 1996.

[24] B. Castaing and B. Dubrulle, "Fully Developed Turbulence: A Unifying Point of View," *J. de Physique II France,* vol. 5, pp. 895-899, 1995.

[25] P. Chainais, "Cascades Log-Infiniment Divisibles et Analyse Multirésolution. Application à l'Étude des Intermittences en Turbulence," PhD dissertation, ENS Lyon, 2001.

[26] A. Arneodo, J. Muzy, and S. Roux, "Experimental Analysis of Self-Similarity and Random Cascade Processes: Application to Fully Developed Turbulence Data," *J. de Physique II France,* vol. 7, pp. 363-370, 1997.

[27] P. Chainais, P. Abry, and J. Pinton, "Intermittency and Coherent Structures in a Turbulent Flow: A Wavelet Analysis of Joint Pressure and Velocity Measurements," *Physics of Fluids,* vol. 11, no. 11, pp. 3524-3539, 1999.

[28] J. Barral and B. Mandelbrot, "Multiplicative Products of Cylindrical Pulses," *Probability Theory and Related Fields,* vol. 124, pp. 409-430, 2002.

[29] J. Muzy and E. Bacry, "Multifractal Stationary Random Measures and Multifractal Random Walks with Log-Infinitely Divisible Scaling Laws," *Physical Rev. E,* vol. 66, 2002.

[30] P. Chainais, R. Riedi, and P. Abry, "Scale Invariant Infinitely Divisible Cascades," *Proc. Int'l Symp. Physics in Signal and Image Processing,* Jan. 2003.

[31] P. Chainais, R. Riedi, and P. Abry, "On Non Scale Invariant Infinitely Divisible Cascades," *IEEE Trans. Information Theory,* vol. 51, no. 3, pp. 1063-1083, 2005.

[32] P. Chainais, R. Riedi, and P. Abry, "Warped Infinitely Divisible Cascades: Beyond Scale Invariance," *Traitement du Signal,* vol. 22, no. 1, 2005.

[33] B. Mandelbrot, "Intermittent Turbulence in Self-Similar Cascades: Divergence of High Moments and Dimension of the Carrier," *J. Fluid Mechanics,* vol. 62, pp. 331-358, 1974.

[34] P. Chainais, "Multi-Dimensional Infinitely Divisible Cascades to Model the Statistics of Natural Images," *Proc. IEEE Int'l Conf. Image Processing,* 2005.

[35] A. Arneodo, F. Argoul, E. Bacry, J.-F. Elezgaray, and J. Muzy, *Ondelettes, Multifractales, et Turbulences.* Diderot, Editeur des Sciences et des Arts, 1995.

[36] B.B. Mandelbrot and J.W. Van Ness, "Fractional Brownian Motion, Fractional Noises and Applications," *SIAM Revs.,* vol. 10, pp. 422-437, 1968.

[37] J. Muzy, E. Bacry, and A. Arneodo, "The Multifractal Formalism Revisited with Wavelets," *Int'l J. Bifurcation and Chaos,* vol. 4, no. 2, pp. 245-301, 1994.

[38] D. Veitch, P. Abry, P. Flandrin, and P. Chainais, "Infinitely Divisible Cascade Analysis of Network Traffic Data," *Proc. IEEE Int'l Conf. Acoustics, Speech, and Signal Processing,* 2000.

[39] E. Bacry, J. Delour, and J. Muzy, "Multifractal Random Walk," *Physical Rev. E,* vol. 64, p. 026103, 2001.

[40] D. Schertzer and S. Lovejoy, "Physical Modeling and Analysis of Rain and Clouds by Anisotropic Scaling Multiplicative Processes," *J. Geophysical Research,* vol. 92, p. 9693, 1987.

[41] F. Schmitt and D. Marsan, "Stochastic Equations Generating Continuous Multiplicative Cascades," *European Physical J. B,* vol. 20, pp. 3-6, 2001.

[42] B.B. Mandelbrot, "Iterated Random Multiplications and Invariance under Randomly Weighted Averaging," *Comptes Rendus (Paris),* vol. 278A, pp. 289-292, 355-358, 1974.

[43] J.-P. Kahane and J. Peyrière, "Sur Certaines Martingales de Benoit Mandelbrot," *Advances in Math.,* vol. 22, pp. 131-145, 1976.

[44] J.-P. Kahane, "Positives Martingales and Random Measures," *Chinese Annals of Math.,* vol. 8B, pp. 1-12, 1987.

[45] W. Feller, *An Introduction to Probability Theory and Its Applications,* vol. 2. John Wiley & Sons, 1966.

[46] E. Bacry and J. Muzy, "Log-Infinitely Divisible Multifractal Processes," *Comm. Math. Physics,* vol. 236, pp. 449-475, 2003.

[47] B. Lashermes, P. Abry, and P. Chainais, "New Insights into the Estimation of Scaling Exponents," *Int'l J. Wavelets, Multiresolution and Information Processing,* vol. 2, no. 4, pp. 497-523, 2004.

[48] B. Rajput and J. Rosinski, "Spectral Representations of Infinitely Divisible Processes," *Probability Theory and Related Fields,* vol. 82, pp. 451-487, 1989.

[49] A. Arneodo, E. Bacry, S. Manneville, and J. Muzy, "Analysis of Random Cascades Using Space-Scale Correlation Functions," *Physical Rev. Letters,* vol. 80, no. 4, pp. 708-711, 1998.

[50] R. Gonzalez and R. Woods, *Digital Image Processing.* Addison-Wesley, 1993.

[51] Y. Gousseau and F. Roueff, "Modeling Occlusion and Scaling in Natural Images," *SIAM J. Multiscale Modeling and Simulation,* pending publication.

[52] A. Srivastava, X. Liu, and U. Grenander, "Universal Analytical Forms for Modeling Image Probabilities," *IEEE Trans. Pattern Analysis and Machine Intelligence,* vol. 24, no. 9, pp. 1200-1214, Sept. 2002.

[53] J.M. Geusebroek, "A Scale-Space Analysis of Multiplicative Texture Processes," *Proc. Third Int'l Workshop Texture Analysis and Synthesis (Texture '03),* M. Chantler, ed., pp. 37-40, 2003.

[54] J.M. Geusebroek, "The Stochastic Structure of Images," *Proc. Fifth Int'l Conf. Scale Space and PDE Methods in Computer Vision,* R. Kimmel, N. Sochen, and J. Weickert, eds., pp. 327-338, 2005.
[55] M. Wainwright and E. Simoncelli, "Scale Mixtures of Gaussians and the Statistics of Natural Images," *Advances in Neural Information Processing Systems,* vol. 12, pp. 855-861, 2000.
[56] M. Wainwright, E. Simoncelli, and A. Willsky, "Random Cascades on Wavelet Trees and Their Use in Analyzing and Modeling Natural Images," *Applied and Computational Harmonic Analysis,* vol. 11, pp. 89-123, 2001.
[57] A.B. Lee, D. Mumford, and J. Huang, "Occlusion Models for Natural Images: A Statistical Study of a Scale-Invariant Dead Leaves Model," *Int'l J. Computer Vision,* vol. 41, no. 1-2, pp. 35-59, 2001.
[58] L. Alvarez, Y. Gousseau, and J. Morel, *The Size of Objects in Natural Images,* vol. 111. Academic Press, 1999.
[59] Z. Chi, "Probability Models for Complex Systems," PhD dissertation, chapter 7, Brown Univ., 1998.
[60] S. Deguy and A. Benassi, "A Flexible Noise Model for Designing Maps," *Vision, Modelling and Visualization,* Nov. 2001.
[61] G. Burd and E. Waymire, "Independent Random Cascades on Galton-Watson Trees," *Proc. Am. Math. Soc.,* vol. 128, pp. 2753-2761, Mar. 2000.
[62] B. Mandelbrot, *The Fractal Geometry of Nature.* W.H. Freeman, 1983.
[63] B. Castaing, "Turbulence: Statistical Approach," *Scale Invariance and Beyond,* B. Dubrulle, F. Graner, and D. Sornette, eds., pp. 225-234. Centre de Physique Les Houches, EDP Sciences-Springer, 1997.
[64] A. Naert, R. Friedrich, and J. Peinke, "A Fokker-Planck Equation for the Energy Cascade in Turbulence," *Physical Rev. E,* vol. 56, p. 6719, 1997.
[65] J. Koenderink, "The Structure of Images," *Biological Cybernetics,* vol. 50, pp. 363-370, 1984.
[66] B. Castaing, "The Temperature of Turbulent Flows," *J. de Physique II France,* vol. 6, pp. 105-114, 1996.
[67] S. Roux, A. Arneodo, and N. Decoster, "A Wavelet-Based Method for Multifractal Image Analysis. III. Applications to High-Resolution Satellite Images of Cloud Structure," *European Physical J. B,* vol. 15, pp. 765-786, 2000.
[68] D. Heeger and J. Bergen, "Pyramid Based Texture Analysis/Synthesis," *Computer Graphics Proc.,* pp. 229-238, 1995.
[69] L.-Y. Wei and M. Levoy, "Fast Texture Synthesis Using Tree-Structured Vector Quantization," *Proc. 27th Ann. Conf. Computer Graphics and Interactive Techniques,* pp. 479-488, 2000.
[70] C. Gallagher and A. Kokaram, "Non Parametric Wavelet Based Texture Synthesis," *Proc. IEEE Int'l Conf. Image Processing,* 2005.
[71] A. Arneodo, E. Bacry, and J. Muzy, "Random Cascade on Wavelet Dyadic Trees," *J. Math. Physics,* vol. 39, no. 8, pp. 4142-4164, 1998.
[72] E.A. Novikov, "Intermittency and Scale-Similarity in the Structure of a Turbulent Flow," *Prikladnaja Matematika i Mechanika J. Applied Math. and Mechanics,* vol. 35, pp. 231-241, 1971, voir aussi Prikladnaja Matematika i Mechanika 35 266-277 (1971).
[73] J. Portilla and E. Simoncelli, "A Parametric Texture Model Based on Joint Statistics of Complex Wavelet Coefficients," *Int'l J. Computer Vision,* vol. 40, pp. 49-71, Oct. 2000.
[74] P. Chainais and J.-J. Li, "Synthèse de Champs Scalaires Multifractals: Application à la Synthèse de Texture," *Proc. 20th Colloquium Groupe de Recherche et d'études du Traitement du Signal et des Images (GRETSI),* 2005.
[75] J.M. Fadili and L. Boubchir, "Analytical Form for a Bayesian Wavelet Estimator of Images Using the Bessel K Form Densities," *IEEE Trans. Image Processing,* vol. 14, pp. 231-240, Feb. 2005.

Pierre Chainais received the BS degree in mathematics in 1995, the degree of agrégation de sciences physiques in 1996, the MSc degree in physics in 1997, and the PhD in physics in 2001 from the Ecole Normale Supérieure de Lyon, France. He joined the University Blaise Pascal at Clermont-Ferrand as a visiting research associate in signal processing in 2002. He is currently an assistant professor of physics and signal processing at University Blaise Pascal. His research interests include self-similar stochastic processes, multifractal analysis, texture synthesis, wavelets, and scaling laws with applications to physical systems (turbulent flows, solar corona, clouds, and so forth). He is a member of the IEEE.